Journal of Zhejiang University-SCIENCE A (Applied Physics & Engineering) 2025 26(4):320-338
www.jzus.zju.edu.cn; www.springer.com/journal/11582
E-mail: jzus_a@zju.edu.cn

Research Article

https://doi.org/10.1631/jzus.A2300639

Effects of the jet fan air velocity response strategy and fire source location on the immersed tunnel fire smoke control

Jianzhong CHEN[1,2], Haining ZHANG[1✉], Liang WANG[1✉], Songlin LIU[1]

[1]*State Key Lab of Coal Mine Disaster Dynamics and Control, Chongqing University, Chongqing 400044, China*
[2]*China Merchants Chongqing Communications Technology Research and Design Institute Co. Ltd., Chongqing 400067, China*

Abstract: Jet ventilation is widely used in the ventilation design of highway and railway tunnels as an important air supply method during tunnel operation and disaster periods. This ventilation method has also been applied for fire control in immersed tunnels. We conduct numerical simulations using computational fluid dynamics (CFD) to study positive ventilation in the upstream and reverse ventilation in the downstream (P-R) for an extra-wide immersed tunnel. The effects of fire source location and jet fan air velocity response strategy on the ceiling temperature decay, carbon monoxide (CO) distribution, and smoke exhaust efficiency were investigated for varying fire source locations. The results show that flames will be tilted to the side of the jet fan with a smaller air velocity. Additionally, the jet fan air velocity should be adjusted based on the relative distance between the fire source and the smoke vent. Among the studied scenarios, the most effective outcome was achieved when the air velocity was adjusted to 25 m/s on the side near the smoke vent. Also in this scenario, the phenomenon of smoke deposition was effectively mitigated and the average smoke exhaust efficiency reached 87%. Moreover, we found that the temperature decay of the tunnel follows an exponential decay law. The temperature decay rate is significantly higher on the side closest to the smoke vent compared to the farther side. This research provides a theoretical basis for smoke control strategies for fires that occur in immersed tunnels.

Key words: Immersed tunnel; Longitudinal temperature decay; Longitudinal carbon monoxide distribution; Tunnel fire; Reversible jet fan air velocity

1 Introduction

With increasing traffic velocities in tunnels and larger amounts of hazardous materials being transported, tunnel accidents are becoming more common. Tunnels are highly-confined structures, so tunnel fires tend to expand rapidly and extensively. In the event of a fire, individuals within the tunnel are exposed to threats such as high temperatures, toxic gases, and potentially even explosions (He et al., 2018; Chen et al., 2020). The ventilation system and smoke exhaust system will form a special flow field inside the tunnel. These factors not only pose significant risks to human lives and property but also compound the challenges of post-disaster evacuation and rescue efforts. Therefore, tunnel fire has been widely considered and studied by many scholars.

Immersed tunnels can avoid impacting original natural environments, and the rapid development of coastal trade and high-grade tunnels has led to cross-river and cross-sea tunnels being widely used. At present, research on immersed tunnel fires has mainly focused on aspects of fire control and fire characteristics. Bai et al. (2019) numerically studied the jet fan performance in urban utility tunnels using Fluent 14.0 and the k-ε turbulence model. They found that airflow velocity was higher upstream of the fire source and that jet fan deflection angles significantly affected the ventilation efficiency. The optimal deflection angle near the fire source was 12° for improved airflow and temperature control. Liu et al. (2016) established a full-size experimental tunnel to conduct a series of fire tests comparing the effects of different smoke vent opening methods on the smoke exhaust efficiency. Their study showed that the smoke exhaust efficiency of two sets

✉ Haining ZHANG, zhn15735219462@163.com
Liang WANG, lw38c@cqu.edu.cn
Liang WANG, https://orcid.org/0000-0001-8927-5796

Received Dec. 18, 2023; Revision accepted May 28, 2024; Crosschecked Mar. 7, 2025

of downstream vents was greater than that of only one set of open vents. Furthermore, Liu et al. (2021) found that the use of supplementary exhaust ducts in immersed tube tunnels can increase the smoke exhaust efficiency from 73% to 98%. Zhang et al. (2022) investigated immersed tunnels with varying aspect ratios, and found that a lateral exhaust vent with an aspect ratio of 1:3 showed the best smoke exhaust performance in immersed tunnels. Similarly, Khalid et al. (2023) investigated the effect of smoke vent aspect ratio, lateral exhaust velocity, and vent spacing on smoke exhaust efficiency using the fire dynamics simulator (FDS) software. Zhang et al. (2023) also found that the installation of inclined smoke barriers can effectively improve the lateral smoke exhaust, and when the inclined smoke barriers are higher or the lateral smoke vents are narrower and higher, there is improved smoke exhaust for small-scale fires.

Fire characteristics in immersed tunnels are also a major focus of research. Xu et al. (2018) established a full-size immersed tunnel model for fire experiments, and found that the smoke layer height distribution in the tunnel conformed to a quadratic polynomial with the goodness of fit being over 95%. In another full-scale modeling experiment, Jiang et al. (2022) constructed a 1:1 tunnel cross-section model with a sidewall smoke exhaust for eight fire tests, and found that the fire plume under the sidewall smoke exhaust system was sloped and the lateral temperature distribution was not uniform; meanwhile, the temperature attenuation in the far-field region still followed an exponential decay pattern. Ming et al. (2023) analyzed the smoke flow pattern of a tilted immersed tunnel fire by using FDS, finding that the temperature and smoke velocity distributions decayed exponentially with the change of slope, and that the smoke exhaust mass flow rate was positively correlated with the exhaust smoke volume.

The gradual increase of thermal stresses within the concrete structure exposed to fire can result in structural damage and make the tunnel unsafe. In long and narrow confined spaces, hot smoke from fires tends to accumulate under the ceiling and form a smoke layer. To develop suitable fire protection measures for tunnels, it is imperative to ascertain the longitudinal temperature distribution beneath the tunnel ceiling. With this in mind, Ingason and Li (2010) developed a formula for calculating the temperature distribution underneath the ceiling of a longitudinally ventilated tunnel through fitting experimental results. Zhao et al. (2018) found that upstream longitudinal temperatures decay faster in longitudinally ventilated tunnels by scaling down the experiments, and found that an increase in longitudinal wind speed exacerbates this difference. Meng et al. (2018) investigated the fire behavior downstream of vehicle blockages and the temperature distribution of fire smoke flow in the near-fire region, as a function of ventilation velocity and blockage rate. Additionally, Tao et al. (2020) investigated the effects of transverse channel opening state, longitudinal velocity, smoke exhaust rate, and fire location on the temperature distribution of an inclined aid station, using 1:10 scale modeling tests. Moving to numerical techniques, Tao et al. (2022) simulated the temperature distribution in a tunnel ceiling under different exhaust airflow and heat release rates for a single-sided centralized smoke tunnel, and found that the upstream and downstream temperature decay patterns differed significantly. Also, Li et al. (2023) developed a computational model for predicting the longitudinal distribution of the maximum smoke temperature rise under the tunnel ceiling, and the results of this model agreed with experimental results. Gao et al. (2024) established another temperature distribution model for the ceiling of a tunnel, taking into account the longitudinal slope factor. Furthermore, Li et al. (2024) found through experimental studies that tunnel blocking significantly affects the peak temperature values, but hardly changes the longitudinal distribution of temperature.

There has also been significant research on smoke flow and control in tunnels employing longitudinal ventilation systems. The critical air velocity is a vital index for controlling fire smoke. Thomas (1958, 1968) introduced the concept of the Froude number of the smoke layer by analyzing the buoyant and inertial forces of the back-layering smoke flow in a tunnel. Further studying the back-layering smoke flow, Thomas (1958, 1968) developed a dimensionless empirical model for the back-layering length of smoke based on the Froude number and derived an expression for the critical longitudinal velocity. Moreover, Oka and Atkinson (1995) considered the influence of tunnel shape, size, and fire source location on smoke flow. Specifically, they modified the empirical formula of critical velocity by utilizing small-scale experimental results. Also, Hu et al.

(2008) proposed a predictive model for back-layering smoke length and critical longitudinal velocity, based on pressure equilibrium equations and the longitudinal smoke temperature attenuation upstream. Li et al. (2010) analyzed the impact of blockage rate on the critical velocity and back-layering length through an experimental method. Weng et al. (2016) categorized tunnels into two groups based on cross-sectional shape factors being greater or less than 1, and developed a predictive model for critical velocity in tunnels with different cross-sectional properties. Also, Ho et al. (2022) investigated the effect of vehicle blockage on the length of smoke backflow, using variables of the shape and configuration of the vehicle blockage, the blockage rate, and the location of the fire. Additionally, He et al. (2023) analyzed the influence of longitudinal fire source location and heat release rate on the induced airflow and smoke movement behavior on both sides of the fire source. They found that symmetric induced airflows would be formed in the vicinity of the fire source induced by thermal pressure, resulting in asymmetric kinetic parameters of the ceiling jet. Chen et al. (2023) investigated the effect of longitudinal fire source location on critical velocity using a T-shaped bifurcated tunnel. Their results showed that the variation of critical velocity with longitudinal fire source position can be classified into two regions: a growth region and a stabilization region.

To minimize casualties and property loss in the event of a fire, it is necessary to ventilate road tunnels. Jet fans have become the preferred technology for road tunnel ventilation systems. They achieve ventilation by inducing airflow in the tunnel, forming a certain air velocity through the injection of high-velocity air from the outlet. Numerous studies have explored the impact of jet fans on tunnel ventilation systems. Chung and Chung (2007) investigated the effect of jet fans on the flow field in road tunnels using numerical simulation. Wang et al. (2012) numerically investigated the effect of the deflection angle of jet fans on tunnel ventilation, and proposed an optimal deflection angle for normal ventilation in curved tunnels. Additionally, Se et al. (2012) investigated the effect of jet fan position on the distribution of airflow velocity and temperature, and Zarnaghsh et al. (2019) studied the effect of airflow generated by a train running at different velocities on the operating parameters of the jet fans, as well as the resulting airflow and pressure drop in tunnels.

However, it is worth mentioning that most existing experimental studies on jet fans use the same upstream and downstream jet wind speeds, and only use positive jet directions. Furthermore, the impact of different air velocity response strategies on fire smoke control in immersed tunnels has not been considered. Meanwhile, the complex structure of immersed tunnels and long evacuation distances make smoke extraction and evacuation difficult. Therefore, the harm of an immersed tunnel fire is generally greater than that of a general tunnel fire. Liu et al. (2021) suggested that installing supplementary exhaust ducts in extra-wide immersed tunnels and using a reasonable longitudinal velocity can significantly improve the efficiency of smoke exhaust. However, most previous numerical studies of longitudinal ventilation based on FDS have used the entire cross-section of the tunnel, which means they assume a uniformly supplied air surface. In real tunnels, fans are installed on the ceiling or sidewalls, and the jet fan generates a high-velocity airflow at the exit area, rather than providing a uniform air supply over the entire tunnel cross-section. We have compared the different operation modes for reversible jet fans and found that the P-R (positive ventilation in the upstream and reverse ventilation in the downstream) operation mode significantly improves exhaust efficiency. Therefore, in this paper, we make a study of the forward-reverse operation mode of jet fans.

Based on this, we propose a strategy for adjusting the upstream or downstream jet fan outlet air velocity based on the distance between the fire source and the smoke vent for fires occurring at different locations in an immersed tunnel. Choosing a reasonable air velocity response strategy provides a theoretical basis for optimizing the jet fan's outlet air velocity.

2 Numerical modeling method

2.1 Theoretical basis

Conducting fire experiments in full-size tunnels requires large material and financial resources. Moreover, there is a possibility of causing damage to the tunnel structure during testing. However, numerical simulations have the advantage of being inexpensive and easy to perform. Therefore, computational fluid dynamics (CFD) methodology is increasingly used for fire simulation in long and narrow spaces. The FDS is

an open-source software package for CFD developed by the National Institute of Standards and Technology, USA (McGrattan et al., 2013). FDS simulation employs large eddy simulation (LES) as a default, which enables modeling of smoke movement. This method provides the most realistic representation of fire and smoke propagation and has successfully solved numerous challenges associated with tunnel fires. Furthermore, the accuracy and validity of computational results from FDS simulations have been substantiated by many experimental results (Gannouni and Maad, 2015).

After a tunnel fire occurs, chemical changes such as fuel combustion satisfy the component conservation theory, and so the movement of smoke and air must also satisfy the three major conservation theorems of fluid dynamics. The main control equations related to FDS are described in Section S1 of the electronic supplementary materials (ESM), and the heat transfer process for a tunnel fire is elaborated on in Section S2 of the ESM.

2.2 Tunnel configurations

To investigate the optimal air velocity response strategy of the jet fans, we utilize an immersed tunnel and jet fan model as shown in Fig. 1. The model is based on the Shenzhen-Zhongshan cross-river corridor's immersed tunnel, which is a two-way eight-lane extra-long submarine highway tunnel. The model measures 350 m in length, with a cross-sectional width of 20 m and a height of 8 m. Concrete is used to construct the model tunnel ceiling, sidewalls, bottom plate, and exhaust ducts. Its constant specific heat is 0.88 kJ/(kg·K), and the constant thermal conductivity is 1.00 W/(m·K). To simulate the environmental conditions in the tunnel,

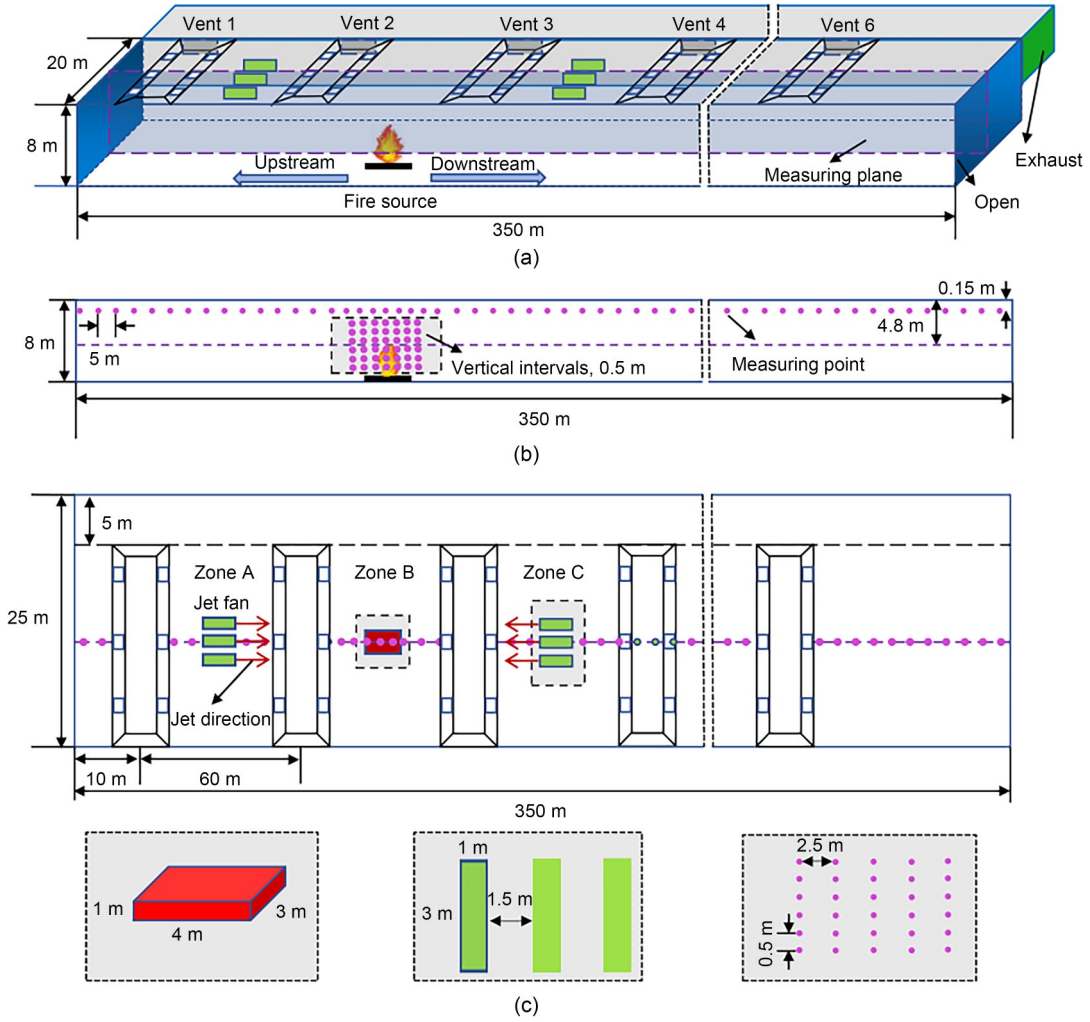

Fig. 1 Schematic of the tunnel model: (a) 3D view; (b) front view; (c) top view

both ends are set as open boundaries. The tunnel's initial ambient temperature is 20 ℃. The fire source is positioned along the tunnel's longitudinal axis, featuring a burner area of 3 m×4 m. Fire heat release rate (HRR) is a crucial parameter for tunnel fire studies, and we choose its value as 50 MW to simulate a severe fire scenario. Heptane (C_7H_{16}) is selected for the reaction type. The mass fraction of fuel converted to carbon monoxide (CO) is 0.006 and the mass fraction of fuel converted to smoke particles is 0.015. The default reaction equation is defined as:

$$C_7H_{16}+10.862O_2 \rightarrow 6.855CO_2+7.993H_2O+0.0214CO+0.1376\text{Soot}.$$

The energy released per unit mass of oxygen is 13100 kJ/kg, so the amount of soot produced per second in a 50 MW fire can be calculated as 16.47 g/s. The ratio of the amount of soot extracted to the amount of soot produced is called the smoke extraction efficiency, and its formula is as follows:

$$\eta = \frac{m_e}{m_p} \times 100\%, \tag{1}$$

where η is the exhaust efficiency (%); m_e is the amount of soot extracted (g/s); m_p is the amount of soot produced (g/s).

To monitor temperature and CO concentrations, a series of measurement points were established along the longitudinal centerline at 0.15 m below the tunnel ceiling. The longitudinal spacing between adjacent measuring points up to 30 m from the fire source is 2.5 m, while the longitudinal spacing of the measuring points in other areas is 5 m. Temperature, CO, and visibility detection surfaces are set in the central longitudinal plane of the tunnel. A supplementary exhaust duct is placed every 60 m in the tunnel and the jet fans are positioned at the center of two supplementary exhaust ducts. One group contains three reversible jet fans, with a fan axis spacing of 2.5 m, a fan length of 3 m, and a diameter of 1 m. In real applications, the outlet air velocity of road tunnel jet fans is typically 20–40 m/s, so in this study, we vary the velocity within this range. A velocity measuring point is placed 4 m in front of the center of the jet fan outlet surface to measure the air velocity. The distance between the center of the jet fan and the entrances of the tunnel in Zones A and C are 40 and 160 m, respectively.

2.3 Fire scenario

We have designed five distinct fire scenarios, where the fire source is positioned at distances of 70, 85, 100, 115, and 130 m from the tunnel entrance. The tunnel is segmented by the supplementary exhaust duct into several zones. The smoke is controlled by adjusting the outlet air velocity of the jet fans in Zones A and C. A total of five different jet fan air velocity response strategies are considered. The direction of fan operation is defined as positive (P, indicated by the symbol "+") from left to right, and negative (R, indicated by the symbol "−") from right to left. Positive ventilation is used for all upstream and reverse ventilation is used downstream (P-R). We hold the air velocity of the jet fan on the far side of the smoke vent constant at 30 m/s. The air velocity of the jet fan on the near side of the smoke vent varies from 30 m/s, with the five air velocities being set to 20, 25, 30, 35, and 40 m/s, respectively. When the fire source deviates from the center of the two smoke vents, the upstream or downstream jet fan outlet air velocity is adjusted according to the distance between the fire source and the smoke vents. The jet fan velocity is held constant on the side where the fire source is farther away from the smoke vent (V_{far}). However, we change the jet air velocity on the side closer to the smoke vent (V_{near}). The specific design conditions are detailed in Section S3 of the ESM. The near side of the smoke vent and the far side of the smoke vent are illustrated in Section S4.

2.4 Grid independence analysis

The grid size significantly affects the accuracy of the FDS calculation results. An excessively large grid size introduces significant errors, while an overly small size can reduce simulation velocity and lead to resource inefficiency. Therefore, to ensure the reliability of the FDS simulation, it is necessary to choose an appropriate grid size. Grid sizes between $D^*/16$ and $D^*/4$ have been widely recognized as effective, where D^* is calculated by the following equation (McGrattan et al., 2013):

$$D^* = \left(\frac{Q}{\rho_\infty C_p T_\infty \sqrt{g}}\right)^{2/5}, \tag{2}$$

where D^* is the characteristic diameter of the fire source (m); Q is the heat release rate of the fire source (kW);

ρ_∞ is the ambient air density (kg/m^3); C_p is the specific heat capacity of ambient air (kJ/(kg·K)); T_∞ is the ambient air temperature (K); g is the gravitational acceleration.

For a 50 MW fire scenario, the characteristic diameter of the fire source is 4.4 m. To ensure the accuracy of the simulation results, we encrypt the grids close to the fire source and the jet fan. To determine an appropriate grid size, we select five grid combinations for independence verification, as shown in Table 1.

The longitudinal temperature distribution for the five grid combination systems and the air velocity variation at the measurement point located 4 m ahead of the jet fan outlet are shown in Fig. 2. The temperature difference in the area near the fire source is the largest under different grid combination systems. Systems A and B exhibit relatively similar temperature profiles, with increases in grid size leading to progressively larger temperature disparities. With regard to velocity change, we can see that Systems A and B exhibit nearly identical velocity trends, showing stable air velocity. Conversely, other grid combination systems display substantial velocity fluctuations. Therefore, in consideration of both temperature and velocity distributions, we select the grid combination System B to strike a balance between calculation accuracy and simulation time. For each fire model, the modeled space is divided into eight regions, as shown in Section S7 of the ESM.

The area within 30 m of the fire source and the area near the jet fan are meshed with small cells of size 0.3125 m×0.25 m×0.25 m. The exhaust duct is divided into cells of size 0.5 m×0.5 m×0.5 m, while the other areas are divided into units of size 0.625 m×0.5 m×0.5 m.

2.5 Scaled model experimental validation

Considering that the tunnel simulated in this study is an immersed tunnel with an extra-wide section, to verify the accuracy of the numerical method, we construct a validation numerical model of the same size of the tunnel. This is based on 1∶15 scaled-down extra-wide immersed tunnel models constructed by other scholars (Wang et al., 2012), and greater detail on this approach is given in Section S6 of the ESM.

Table 1 Grid combination system

Grid system	Grid size		Total cell number
	Near the fire region and the fan region	Other regions	
A	0.25 m×0.25 m×0.25 m	0.5 m×0.5 m×0.5 m	875840
B	0.3125 m×0.25 m×0.25 m	0.625 m×0.5 m×0.5 m	711872
C	0.357 m×0.25 m×0.25 m	0.714 m×0.5 m×0.5 m	629888
D	0.357 m×0.357 m×0.25 m	0.714 m×0.714 m×0.5 m	433552
E	0.5 m×0.5 m×0.5 m	1.0 m×1.0 m×1.0 m	166300

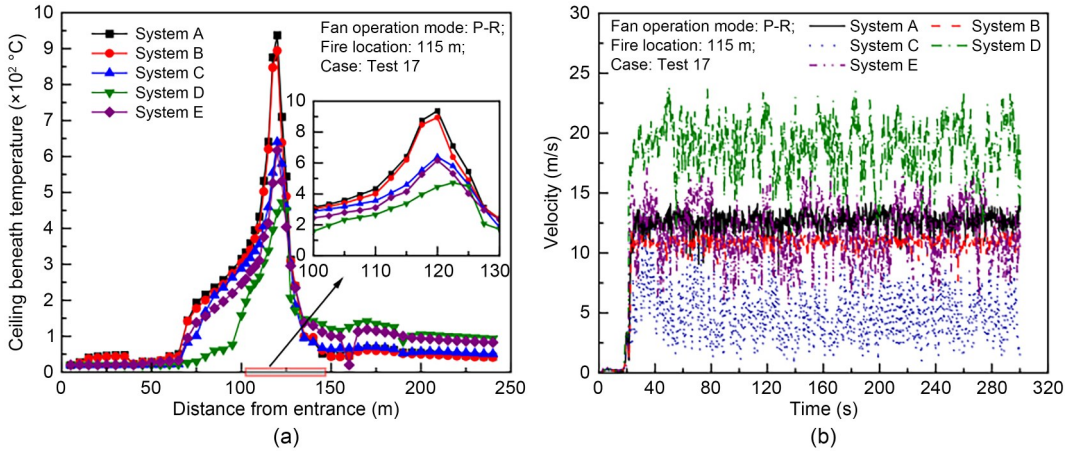

Fig. 2 Grid independence analysis: (a) longitudinal temperature distribution; (b) velocity variation with time. References to color refer to the online version of this figure

3 Results and discussion

3.1 Temperature distribution

To ensure the accuracy of the numerical experiments, we set each test to last 300 s. Data monitoring is conducted throughout the numerical experiment to identify significant fluctuations. As shown in Fig. 3, approximately 150 s after the initiation of the fire source combustion, both the temperature and velocity converge towards constant levels. This signifies that the combustion has become stable. Therefore, we use the average values across the time interval from 200 to 300 s, instead of the stable stage.

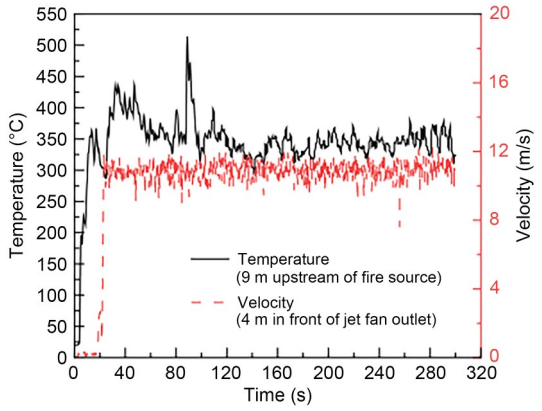

Fig. 3 Temperature and velocity variation with time

3.1.1 Vertical distribution of temperatures downstream of the fire source

Fig. 4 shows the vertical distribution of downstream temperature for varying fire source positions and jet fan air velocity response strategies. The downstream vertical temperature increases with the increase in height. Across the different working scenarios, there is a gradual rise in the range of 2.3–5.3 m, and an accelerated rise in the range of 5.3–7.3 m. This is because the high-temperature smoke causes a large amount of heat to accumulate at the top of the tunnel due to buoyancy. As a result, the upper levels exhibit significantly higher smoke temperatures compared to the lower levels. When the fire source is positioned beneath the smoke vent, the air velocity response strategy of the jet fan has a more significant impact on the vertical temperature. When X<100 m (X is the location of the fire in the longitudinal direction of the tunnel), increasing the air velocity of the upstream jet fan leads to a gradual increase in downstream vertical temperatures. Conversely, for X>100 m, increasing the downstream jet fan air velocity results in a gradual reduction in downstream vertical temperatures. This phenomenon can be attributed to the high-velocity jet's ability to drive a larger volume of smoke causing the accumulation of high-temperature smoke in the flow direction.

3.1.2 Longitudinal temperature distribution

After the fire smoke in the tunnel is heated, it spreads rapidly with the fire plume hitting the ceiling above the fire source. The flame temperature distribution in the tunnel plays a pivotal role in dictating the rate of both smoke diffusion and deposition. In addition, the tunnel ceiling is particularly vulnerable to damage compared to other tunnel components. Therefore, the longitudinal temperature of the tunnel ceiling is an important indicator for studying tunnel fires.

Fig. 5 illustrates the longitudinal temperature field of a fire transitioning into the stable stage with varying positions and jet fan air velocity response strategies. When the upstream jet fan's air velocity is greater than that of the downstream jet fan, the flame inclines downstream. Conversely, when the upstream jet fan's air velocity is lower than that of the downstream jet fan, the flame tilts upstream. Thus, there is a phenomenon where the flame will tilt to the side with lower air velocity. This behavior is attributed to the action of the high-velocity jet, which increases the oxygen concentration and consequently sustains the combustion process. As oxygen flows in the direction of the jet, it also drives the movement of the flame, which manifests itself as a change in the shape of the flame. Therefore, the flame will tilt to the side with lower air velocity.

It can be seen from Figs. 5a and 5b that an increase in the air velocity of the upstream jet fan results in significant downstream dispersion of the smoke. As a result, the upstream high-temperature smoke-spreading distance gradually decreases, while the settling of smoke downstream becomes more pronounced. Therefore, the thickness of the downstream high-temperature smoke layer increases significantly. In addition, increasing the downstream jet fan air velocity can cause severe upstream smoke settling. This occurs because the jet fan can manage the smoke on the side of the fire source when the air velocity is high. However, when the air velocity becomes excessively high, it will increase the degree of airflow disorder. The layered attachment of smoke is destroyed

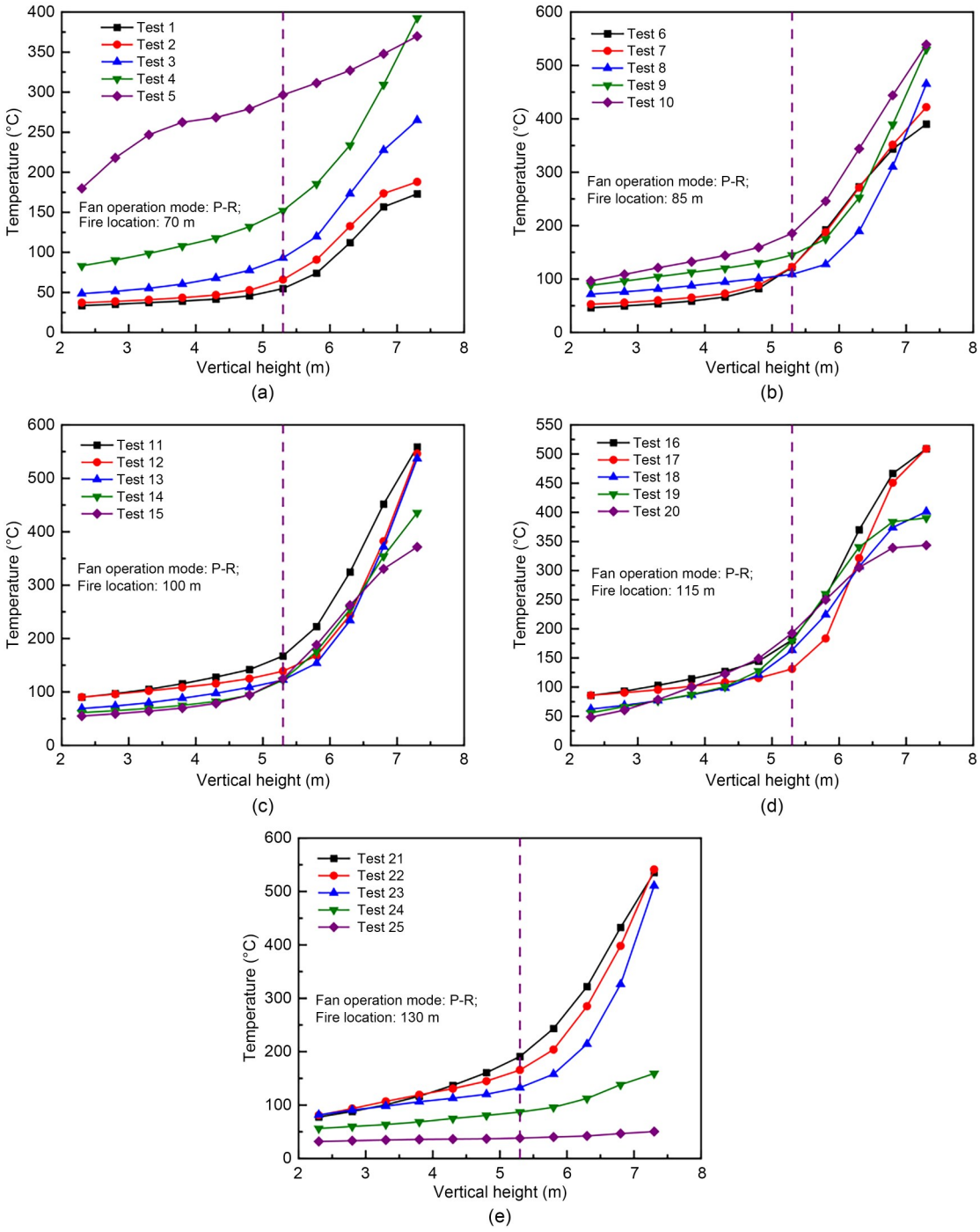

Fig. 4 Vertical distribution of downstream temperature with different fire locations: (a) X=70 m; (b) X=85 m; (c) X=100 m; (d) X=115 m; (e) X=130 m

in advance, which makes the smoke settle prematurely. The tunnel section is filled with smoke in advance. Therefore, when the jet fan adopts the forward and reverse operation mode, appropriately reducing the air velocity of the jet fan on the near side of the smoke vent can effectively mitigate the smoke settling phenomenon.

Fig. 6 depicts the longitudinal distribution of ceiling temperature for varying fire source positions and air velocity response strategies. Due to the asymmetrical placement of smoke vents on either side of the fire source, the jet velocities of the upstream and downstream jet fans are different. Therefore, the maximum

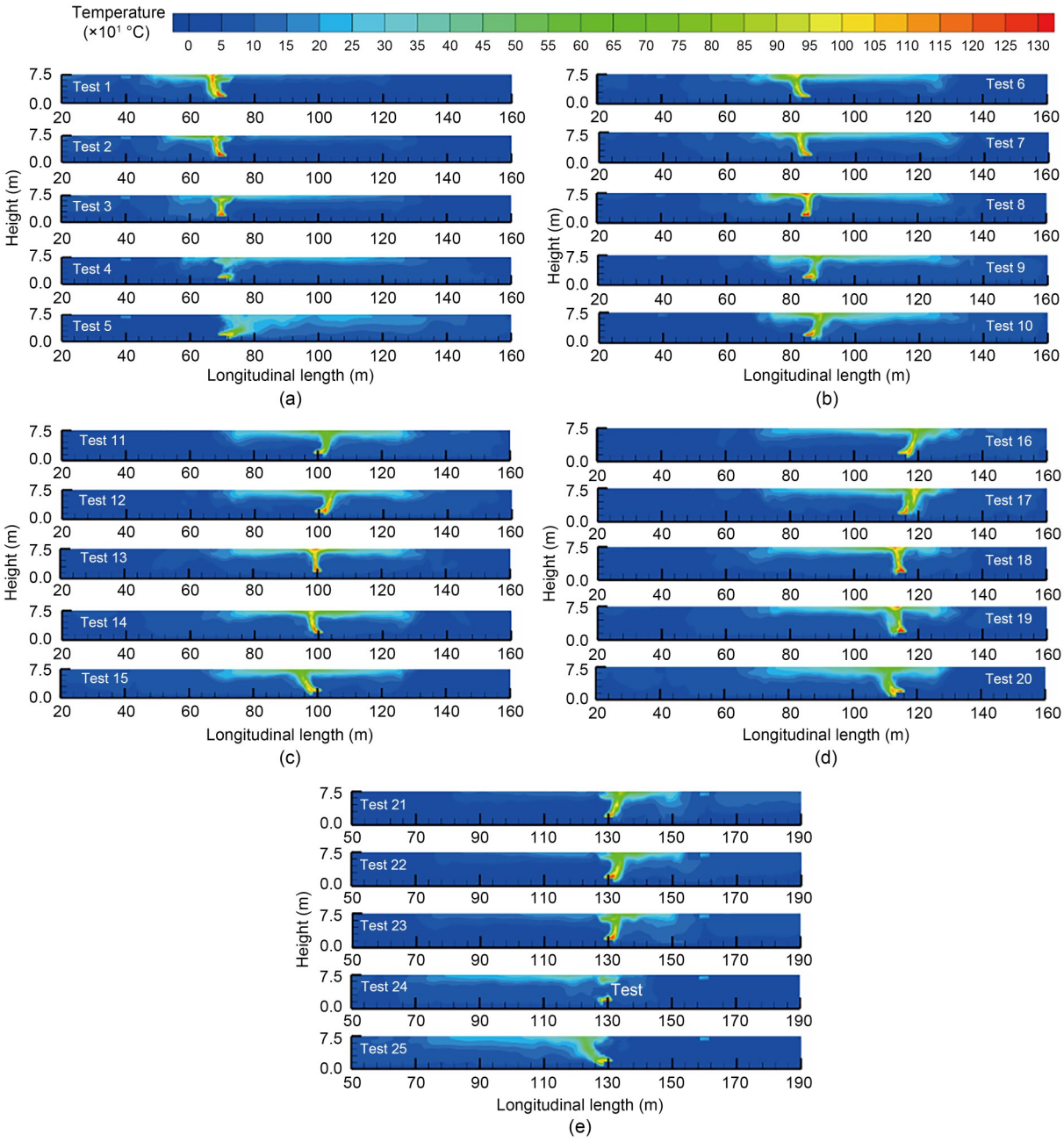

Fig. 5 Temperature slices with different jet fan air velocity combinations and different fire locations: (a) *X*=70 m; (b) *X*=85 m; (c) *X*=100 m; (d) *X*=115 m; (e) *X*=130 m

temperature in the ceiling area does not necessarily occur directly above the fire source, but will occur relatively close to the fire. Overall, the temperature variation across different operating conditions is minimal. The ceiling temperature exhibits a rapid decline from its peak values and then decreases slowly in the area far from the fire. This trend reflects a longitudinal attenuation of ceiling temperatures. In Test 1, the ceiling temperature decreased from 488 to 196 ℃ as the distance from the fire source increased from 0 to 5 m. When the distance extended from 10 to 15 m, the ceiling smoke temperature changed from 172 to 161 ℃. This is because a substantial volume of smoke generated by the tunnel fire flows along the longitudinal direction. During the process of smoke transportation, the smoke interacts with cold air and heat exchange occurs. At the same time, a large amount of heat will be lost to the wall and the surrounding cold environment.

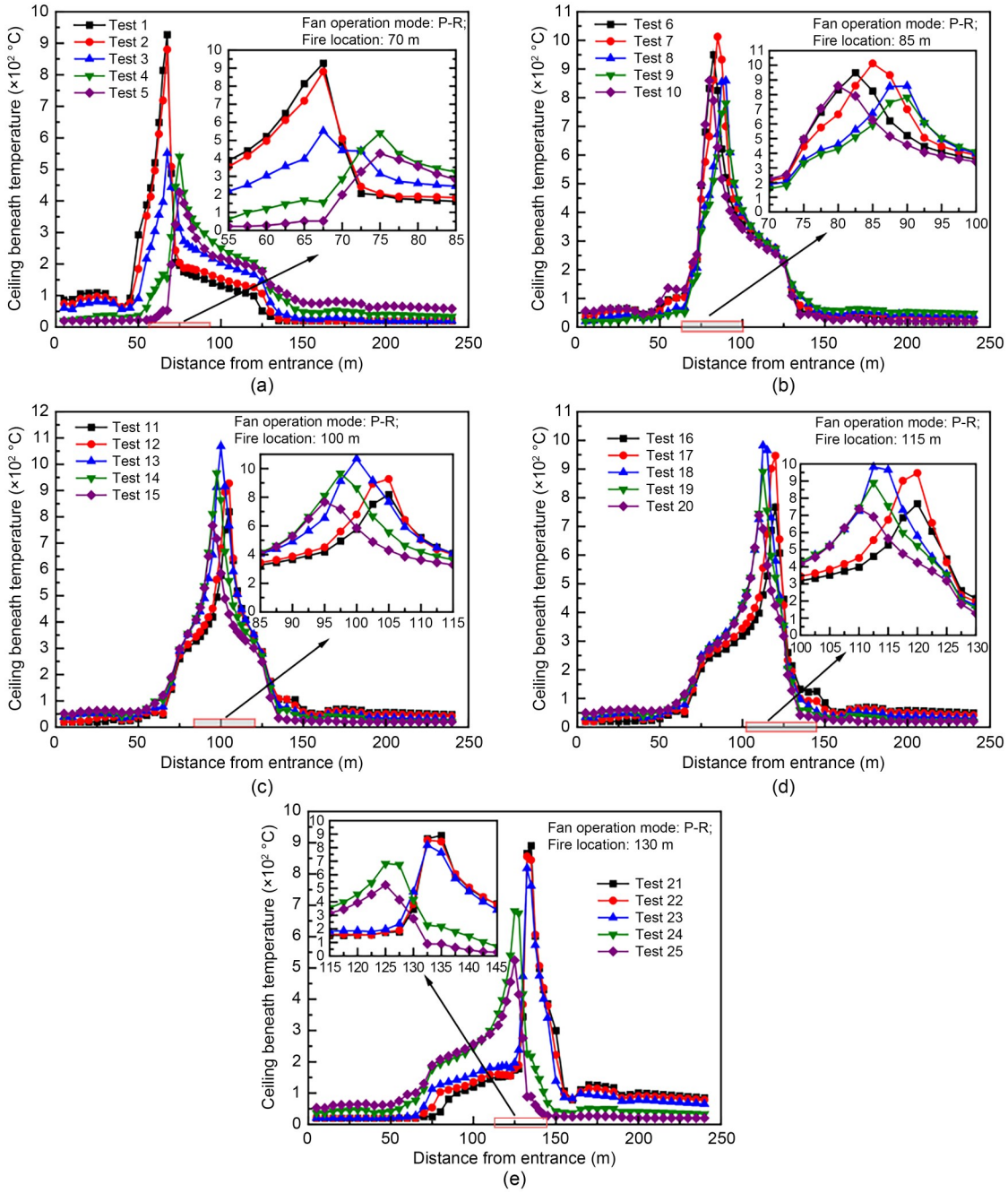

Fig. 6 Longitudinal distribution of tunnel ceiling temperature with different fire locations: (a) X=70 m; (b) X=85 m; (c) X=100 m; (d) X=115 m; (e) X=130 m

These factors contribute to the gradual temperature decline.

The location of the fire source had a significant influence on the longitudinal temperature distribution in the ceiling. When the fire source was centered between the two smoke vents (X=100 m), the ceiling's longitudinal temperature distribution was symmetric. Moreover, the upstream and downstream temperature decay rates were similar. When X<100 m, the temperature distribution curve became inclined, and the upstream temperature decay rate was significantly greater than the downstream temperature decay rate. Conversely, when X>100 m, the downstream temperature decay rate greatly exceeded the upstream temperature decay rate. The above phenomenon indicates that the temperature decay rate is faster on the side closer to the

smoke vent. In addition, there was a sudden drop in ceiling temperature near the smoke vent. This is because the entrainment between the hot smoke near the vent and the colder air in the lower layer is stronger, and the convective heat transfer between the hot smoke and the cold air is more intense. Therefore, the temperature attenuates faster on the near side of the smoke vent.

The influence of the air velocity matching mode of the upstream and downstream jet fans on the ceiling's longitudinal temperature distribution is also significant. The different air velocities of the upstream and downstream jet fans result in varying degrees of flame inclination, and thus influence the flame hitting the tunnel ceiling. Therefore, the position of the highest observed temperature changes. When the fire source is not directly beneath the smoke vent, the maximum temperature difference near the fire source can reach up to 500 ℃ for different jet fan air velocity combinations. In contrast, the maximum temperature difference in the far fire area is less than 50 ℃. Overall, the influence of the jet fan air velocity response strategy on the ceiling temperature is mainly realized in the area near the fire source. However, when the fire source is located directly beneath the smoke vent (X=70 or 130 m), the jet fan's air velocity response strategy significantly impacts the entire ceiling temperature. The maximum temperature difference can reach 800 ℃ in the near fire zone, and 90 ℃ in the far fire zone. When X<100 m, an increase in the upstream jet fan's air velocity results in a gradual decrease in the upstream ceiling temperature and a corresponding increase in the downstream ceiling temperature. When X>100 m, an increase in the downstream jet fan's air velocity leads to a gradual increase in the upstream ceiling temperature and a decrease in the downstream ceiling temperature. This is because after the jet fan injects a high-velocity jet, entrainment will occur between the high-velocity jet and the surrounding gas. The high-velocity jet longitudinally drives the high-temperature smoke to flow along the jet direction. It is worth noting that the critical velocity for a 50 MW fire is about 3.5 m/s. Furthermore, we observed that the smoke back-layering phenomenon occurred in almost all studied conditions. This shows that when high-velocity jets are generated upstream and downstream in opposite directions, the velocity in the tunnel is lower than 3.5 m/s, and smoke cannot be prevented from spreading upstream.

3.1.3 Temperature decay analysis

The diffusion process of the smoke, as driven by thermal buoyancy in the tunnel space, can be divided into four regions as shown in Section S7 of the ESM: the free-rising plume stage (I), radial diffusion stage (II), transition stage (III), and one-dimensional diffusion stage (IV) (Hu et al., 2005).

For the smoke in the one-dimensional diffusion stage, the continuity equation is:

$$\frac{\mathrm{d}\dot{m}}{\mathrm{d}x}=\rho_{\mathrm{a}}\omega_{\mathrm{e}}B, \tag{3}$$

where $\dot{m}$ is the mass flow of smoke (kg/s); ρ_{a} is ambient air density (kg/m^3); ω_{e} is the entrainment velocity (m/s); B is the interface width between smoke layer and fresh air (m); x is the distance to the fire source (m).

The energy equation is:

$$\frac{\mathrm{d}}{\mathrm{d}x}(c_{\mathrm{p}}\dot{m}T)=c_{\mathrm{p}}\rho_{\mathrm{a}}\omega_{\mathrm{e}}BT_{\mathrm{a}}+\alpha D(T-T_{\mathrm{a}}), \tag{4}$$

where c_{p} is the specific heat capacity (J/(kg·K)); T is the temperature (K); T_{a} is the tunnel ambient temperature (K); α is the heat transfer coefficient (W/(m^2·K)); D is the contact length between the section circumference of the smoke layer and the tunnel wall (m).

Hu et al. (2005) simplified the above equations to obtain a theoretical formulation describing the decay of smoke temperature in a one-dimensional diffusion region:

$$\frac{\Delta T_x}{\Delta T_{\mathrm{r,single}}}=\frac{T_x-T_{\mathrm{a}}}{T_{\mathrm{r}}-T_{\mathrm{a}}}=\mathrm{e}^{\frac{-k(x-x_{\mathrm{r}})}{H}}, \tag{5}$$

where x_{r} is the starting position of the one-dimensional diffusion zone (m); $\Delta T_{\mathrm{r,single}}$ is the single-exponential correlation reference temperature, defined by Hu et al. (2005) as the smoke temperature at the starting position of the one-dimensional diffusion zone (ΔT_{r}); ΔT_x is the temperature rise at a distance of x from the reference point (K); k is the temperature attenuation coefficient; H is the tunnel height (m); T_{r} is the temperature at the starting position of the one-dimensional diffusion zone (K); T_x is the temperature at a distance of x from the reference point (K).

Li et al. (2012) conducted a numerical investigation on the smoke temperature distribution of rectangular

cross-section tunnels with aspect ratios ranging from 0.5 to 2.0 under natural ventilation conditions. It was found that there was a significant difference in the fire smoke temperature decay rate between tunnels with an aspect ratio greater than 1 and tunnels with an aspect ratio less than 1. They proposed a piecewise fitting relationship for predicting smoke attenuation in tunnel fires with different aspect ratios:

$$\Delta T_x = \begin{cases} \Delta T_{\mathrm{ref}} \mathrm{e}^{-0.00733\frac{x}{d}}, & R_{\mathrm{a}} \leqslant 1, \\ \Delta T_{\mathrm{ref}} \mathrm{e}^{-0.00406\frac{x}{d}}, & R_{\mathrm{a}} > 1, \end{cases} \tag{6}$$

where ΔT_{ref} is the temperature rise at the reference point (K); d is the hydraulic diameter of the smoke layer (m); R_{a} is the aspect ratio.

It is worth noting that most of the previous studies are based on natural ventilation conditions and do not apply to longitudinal ventilation conditions. Ingason and Li (2010) conducted an experimental study on smoke temperature distribution in a longitudinal ventilation model tunnel. A fitting formula for the double exponential function was proposed:

$$\frac{\Delta T_x}{\Delta T_{\mathrm{r,double}}} = 0.57\mathrm{e}^{-0.13\frac{x}{H}} + 0.43\mathrm{e}^{-0.021\frac{x}{H}}, \tag{7}$$

where $\Delta T_{\mathrm{r,double}}$ is the reference temperature of double exponential correlation, which is defined by Ingason and Li (2010) as the highest smoke temperature directly above the fire source. To eliminate the influence of tunnel size on the attenuation coefficient, the dimensionless distance x/H is introduced.

Ji et al. (2019) studied the influence of fire source shape on smoke movement and temperature distribution in tunnels by numerical simulation. The longitudinal temperature attenuation model is proposed as follows:

$$\frac{\Delta T_x}{\Delta T_{\mathrm{st}}} = 0.559\mathrm{e}^{-0.123\frac{(x-x_{\mathrm{st}})}{H_{\mathrm{b}}}} + 0.417, \tag{8}$$

where ΔT_x is the temperature rise under the tunnel ceiling (K); ΔT_{st} is the temperature rise at the reference point (K); x_{st} is the location of the start of the one-dimensional phase (m); H_{b} is the ceiling gap at the top of the fuel (m).

$$\frac{\Delta T_x}{\Delta T_{\mathrm{st}}} = A\mathrm{e}^{-k\frac{(x-x_{\mathrm{st}})}{H_{\mathrm{b}}}} + C, \tag{9}$$

where A and C are coefficients in the temperature decay model.

Summarizing and analyzing the previous studies on the longitudinal decay of ceiling temperature, it becomes evident that the law of temperature decay can be described in three exponential functions:

$$\frac{\Delta T_x}{\Delta T_{\max}} = \begin{cases} \mathrm{e}^{-k(x-x_{\mathrm{r}})}, \\ A\mathrm{e}^{-k\frac{x-x_{\mathrm{r}}}{H}} + C, \\ E\mathrm{e}^{-k_1\frac{x-x_{\mathrm{r}}}{H}} + F\mathrm{e}^{-k_2\frac{x-x_{\mathrm{r}}}{H}}, \end{cases} \tag{10}$$

where $\Delta T_{\max}$ is the maximum temperature rise; E and F are coefficients in the temperature decay model; k_1 and k_2 are temperature attenuation coefficients.

3.1.4 Temperature decay beneath the tunnel ceiling

In order to establish the ceiling temperature decay model, the highest smoke temperature near the fire source is used as the reference temperature, designating the location of the highest temperature as the reference point. According to the analysis in Section 3.1.2, the ceiling smoke temperature decreases exponentially with the horizontal distance. Therefore, the data of dimensionless temperature and dimensionless distance are fitted using Eq. (8). Figs. 7 and 8 display the relationship between dimensionless smoke temperature and dimensionless horizontal distance, upstream and downstream of the fire source, respectively. As the dimensionless distance increases, the dimensionless temperature rises initially, then decreases sharply, and finally decreases slowly and reaches a steady state. When X<130 m, the upstream dimensionless temperature variations do not exhibit significant sensitivity to changes in jet fan collocation mode, indicating that the dimensionless temperature rise is independent of the jet fan air velocity. The correlation coefficients for the model fitting of upstream temperature decay for different operating conditions ranged from 0.94–0.97.

Similarly, the ceiling temperature in the tunnel downstream of the fire source displayed an exponential decay pattern, and all correlation coefficients for the fitted functions exceeded 0.93. The upstream and downstream fitting results for dimensionless temperature curves are shown in Tables 2 and 3, respectively. It is worth noting that the temperatures in Figs. 7e and 8a also conform to an exponential decay law. However, there is a more pronounced divergence in dimensionless

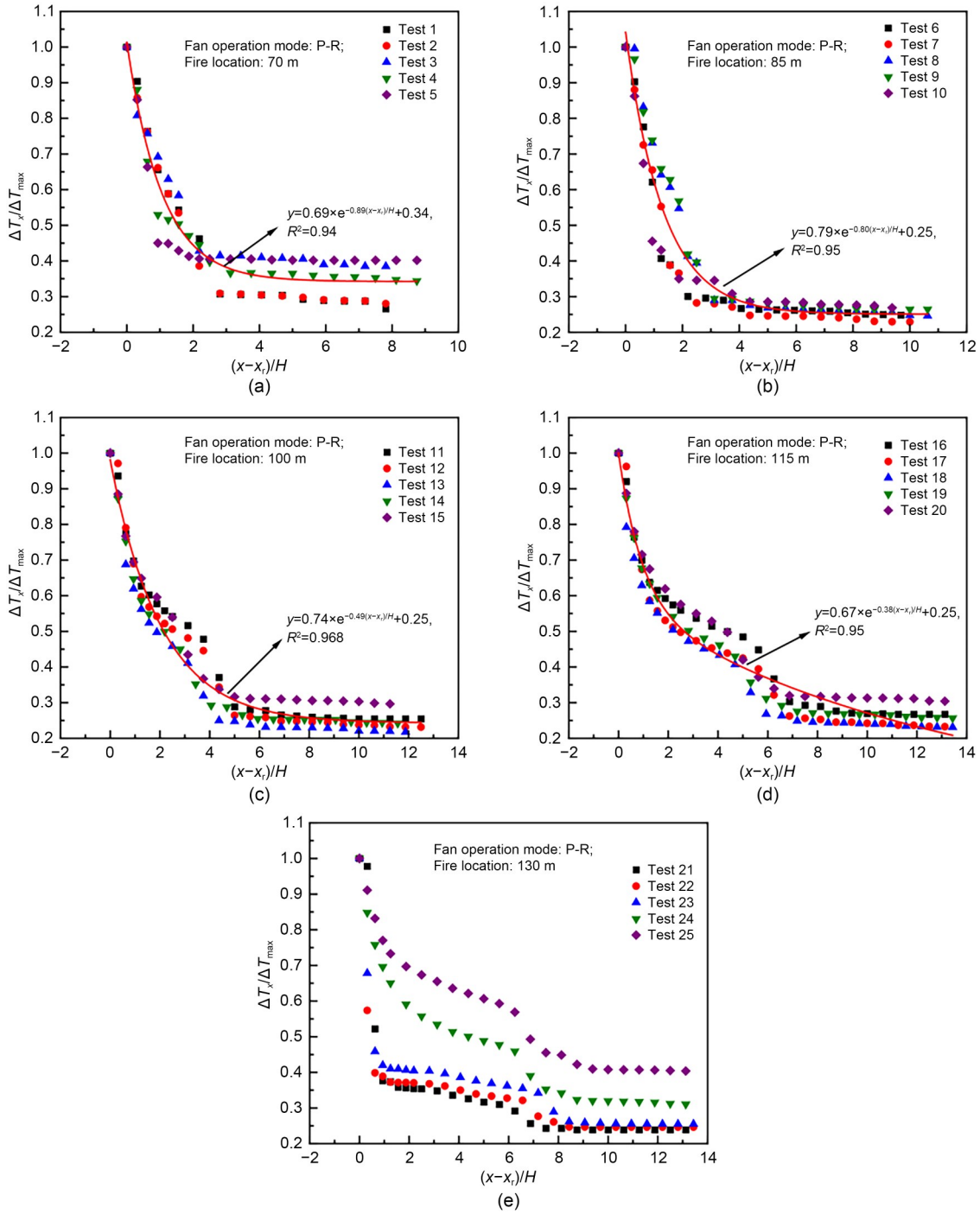

Fig. 7 Correlation between upstream $\Delta T_x/\Delta T_{max}$ and $(x-x_r)/H$ of fire source in different operating conditions: (a) X=70 m; (b) X=85 m; (c) X=100 m; (d) X=115 m; (e) X=130 m

temperature downstream at X=70 m, and a greater disparity upstream at X=130 m. This phenomenon can be attributed to the fire source being located just below the smoke vent and near one side of the jet fan. The interaction between the longitudinal ventilation of the jet fan and the mechanical smoke exhaust causes this difference. Therefore, we exclude these two special cases from further analysis of longitudinal temperature decay.

Based on the above analysis, we further dissect the temperature decay from two perspectives: the near side of the smoke vent and the far side of the smoke

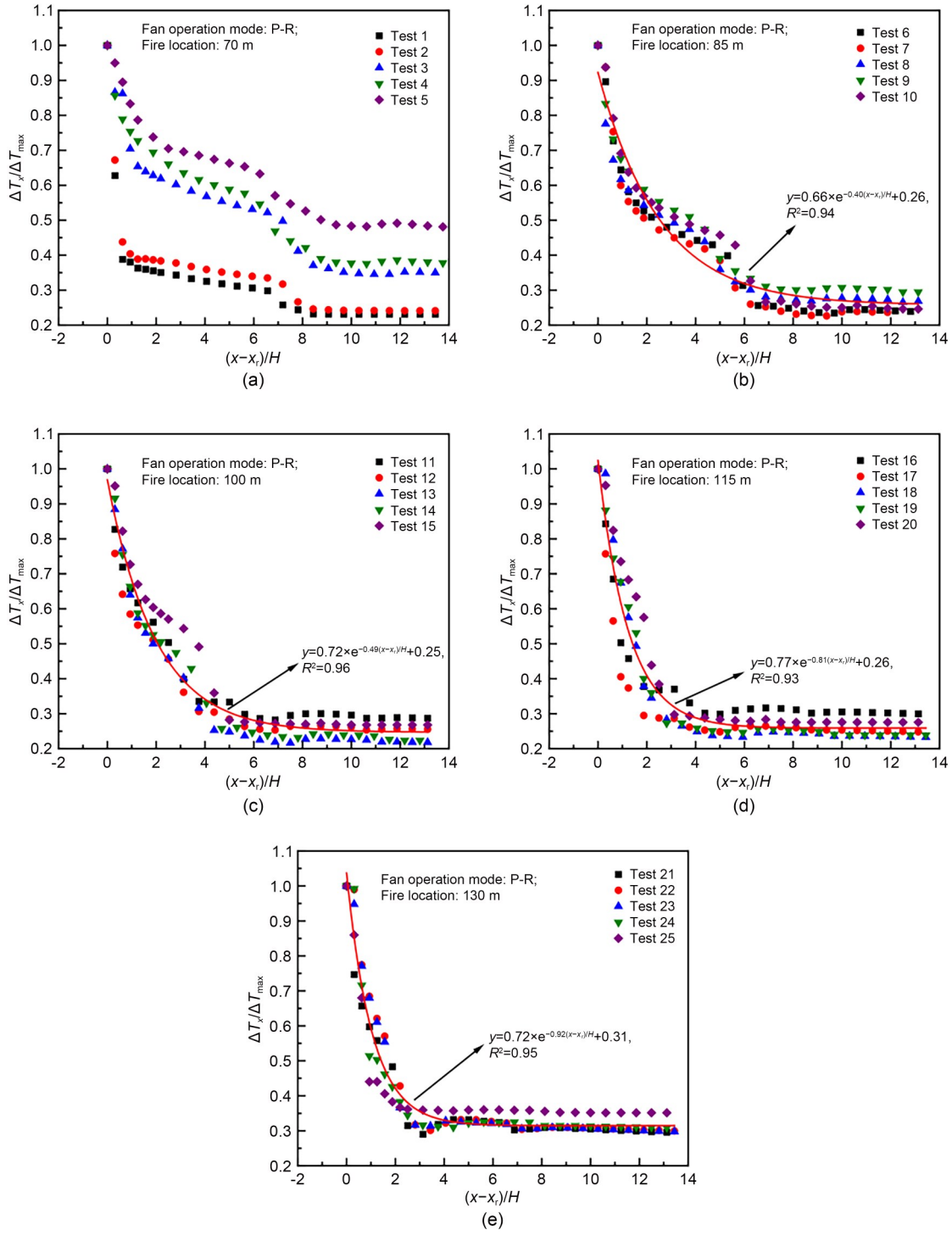

Fig. 8 Correlation between downstream $\Delta T_x/\Delta T_{max}$ and $(x-x_r)/H$ of fire source in different operating conditions: (a) X=70 m; (b) X=85 m; (c) X=100 m; (d) X=115 m; (e) X=130 m

vent. The correlation coefficient of curve fitting is above 0.93, and the jet fan air velocity response strategy has minimal impact on this value. By averaging the coefficients A, C, and k, we can derive a piecewise equation for the longitudinal temperature decay beneath the tunnel ceiling for various fire source positions and jet fan air velocity response strategies. This equation is:

$$\frac{\Delta T_x}{\Delta T_{\max}} = \begin{cases} 0.74\mathrm{e}^{-0.86\frac{X-X_t}{H}}+0.29, & \text{near side of the smoke vent,} \\ 0.70\mathrm{e}^{-0.44\frac{X-X_t}{H}}+0.25, & \text{far side of the smoke vent.} \end{cases} \tag{11}$$

It can be seen from the attenuation curve that the upstream and downstream temperature decay rates are different. When the fire source is located in the center of the two smoke vents, the difference between the two decay curves is minimal. However, as the fire source deviates from the central position, the temperature decay rate on the near side of the smoke vent is significantly higher than that on the far side. This is because the entrainment effect of the smoke vent is stronger as the distance from it decreases. As a result of the combined influence of the exhaust air volume and jet fan, a substantial accumulation of smoke occurs on the near side of the smoke vent.

Table 2 Fitting results for upstream dimensionless temperature rise curves

Case	A	k	C	R^2
X=70 m	0.69	0.89	0.34	0.94
X=85 m	0.79	0.80	0.25	0.95
X=100 m	0.74	0.49	0.25	0.97
X=115 m	0.67	0.38	0.25	0.95
X=130 m	–	–	–	–

Table 3 Fitting results for downstream dimensionless temperature rise curves

Case	A	k	C	R^2
X=70 m	–	–	–	–
X=85 m	0.66	0.40	0.26	0.94
X=100 m	0.72	0.49	0.25	0.96
X=115 m	0.77	0.81	0.26	0.93
X=130 m	0.72	0.92	0.31	0.95

3.2 CO concentration distribution

Research has demonstrated that toxic gases pose a significant risk to human safety during fires. Specifically, CO poisoning is responsible for approximately half of all fire-related fatalities. Therefore, it is important to study the transmission characteristics of CO during tunnel fires.

Fig. 9 describes the longitudinal distribution of CO concentration for different fire locations and jet fan air velocities. As the distance from the fire source increases, the CO concentration gradually decreases. The CO concentration near the fire source decreased rapidly and then decreased slowly. In Test 1, the CO concentration in the ceiling decreased from 100 to 31 μmol/mol when the distance from the fire source was increased from 0 to 5 m. Then, the CO concentration in the ceiling changed from 31 to 26 μmol/mol when the distance was increased from 5 to 10 m. This is attributed to the air entrainment during the smoke diffusion process, which gradually reduces the CO concentration. When X=100 m, the CO concentration in the ceiling exhibits a symmetrical distribution. The air velocity of the jet fan significantly influences the CO concentration when the fire source is directly below the smoke vent. However, when the fire source is not directly below the smoke vent, the jet fan's air velocity only has a substantial impact on the CO concentration in the ceiling near the fire source, while the concentration in the area far from the fire is almost the same. This phenomenon indicates that the interaction between the smoke vent and the jet fan is stronger when the fire source is directly below the smoke vent. Notably, a significant decrease in CO concentration is observed at the smoke vent. This is due to the strong entrainment of the smoke vent on the hot smoke and the cooler air below, which dilutes the CO concentration.

3.3 Smoke exhaust efficiency

Fig. 10 shows the smoke exhaust efficiency of different jet fan air velocity combinations in varying fire source locations. When the air velocities of both upstream and downstream jet fans are the same, the smoke exhaust efficiency remains consistently high. The minimum smoke exhaust efficiency is 84%, and the maximum reaches 96%. When the air velocity of the jet fan on the near side of the smoke vent is less than 30 m/s, increasing the air velocity of the jet fan effectively improves the smoke exhaust efficiency. However, if the jet fan air velocity is greater than 30 m/s, increasing it further will decrease the smoke exhaust efficiency. This is because the jet fan air velocity reaches a certain optimal value, and continuing to increase the air velocity will strengthen the high-velocity jet and promote part of the smoke to propagate along the jet direction. Then, only part of the smoke will gather between the two smoke vents. Therefore, increasing the air velocity at this point will reduce the exhaust efficiency.

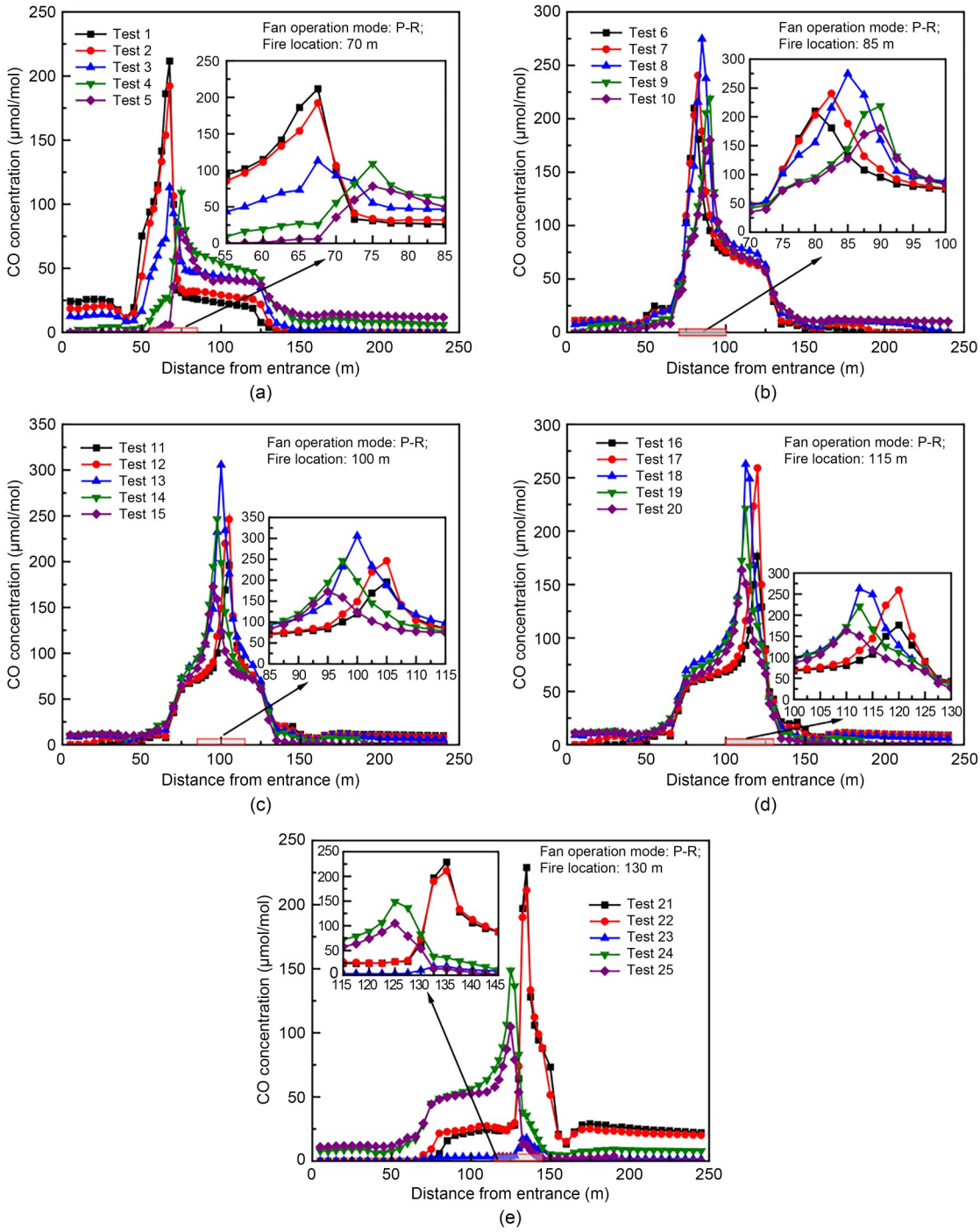

Fig. 9 Longitudinal distribution of CO concentration in the tunnel ceiling for different operating conditions: (a) *X*=70 m; (b) *X*=85 m; (c) *X*=100 m; (d) *X*=115 m; (e) *X*=130 m

In addition, if the air velocity of the jet fan on the near side of the smoke vent is adjusted to 25 m/s, then the smoke exhaust efficiency is lower only when the fire source was located at *X*=130 m, reaching a mere 73%. This is because the fire source is located just below the right smoke vent, and the upstream positive airflow pushes the hot smoke downstream. As a result, a significant amount of smoke accumulates directly downstream without being discharged through the smoke vent. However, the smoke exhaust efficiency can reach almost 90% when the fire occurs in other locations. The average smoke exhaust efficiency remains

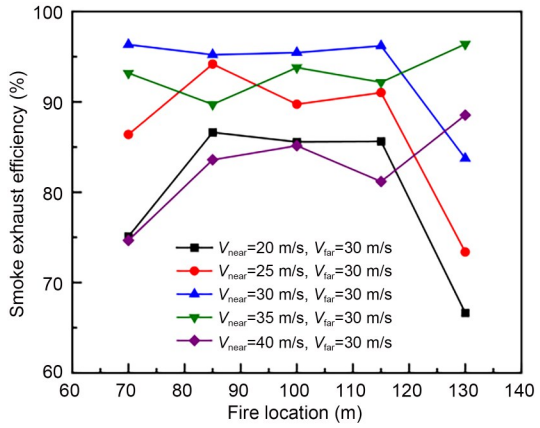

Fig. 10 Smoke exhaust efficiency with different jet fan air velocities for different fire source locations

high at 87%. These findings demonstrate that properly reducing the air velocity of the jet fan on the near side of the smoke vent not only effectively mitigates the smoke settling phenomenon, but also maintains a high level of exhaust efficiency.

4 Conclusions

In this study, the combinations of five relative fire source locations (70, 85, 100, 115, and 130 m) and five jet fan operating conditions in an immersed tunnel were investigated numerically to determine the influences of fire location and jet velocity on ceiling temperature decay, CO distribution, and smoke exhaust efficiency. The following main conclusions are drawn:

(1) The fire's flame will tilt to the side where the jet fan's air velocity is smaller. The velocity of the jet fan near the smoke vent should be regulated in accordance with the distance between the fire source and the smoke vent. Appropriate reduction of the air quantity pushed by the jet fan near the smoke vent can effectively mitigate the phenomenon of smoke settling.

(2) The temperature decay in the tunnel ceiling follows an exponential decay law. The temperature decay rate of the near side of the smoke vent is significantly higher than that of the far side. Accordingly, we proposed temperature decay models of the near side and far side of the smoke vents. The models suggested that there is a sudden drop in ceiling temperature and CO concentration at the smoke vent location.

(3) For the selected operating conditions, the jet fan air velocity of 25 m/s on the near side of the smoke vent is ideal. The average smoke exhaust efficiency was 87% for this setting, and the maximum smoke exhaust efficiency was also high at 95%.

From the results of this study, we propose that the air velocity of the jet fan near the exhaust vent should be 25 m/s. This provides a reference for fire control practices in tunnels with similar geometries. However, it should be noted that we did not consider the influence of the transverse installation spacing and installation height of the jet fan. In the future, the impact of these factors on tunnel fires should be investigated to strengthen these smoke control strategies in immersed tunnels.

Author contributions

Jianzhong CHEN designed the research. Liang WANG wrote the first draft of the manuscript. Songlin LIU helped to organize the manuscript. Haining ZHANG revised and edited the final version.

Conflict of interest

Jianzhong CHEN, Haining ZHANG, Liang WANG, and Songlin LIU declare that they have no conflict of interest.

References

Bai ZP, Li YF, Li JM, 2019. Numerical study the performance of jet fans in utility tunnel ventilation. International Conference on Intelligent Transportation, Big Data & Smart City, p.36-38. https://doi.org/10.1109/ICITBS.2019.00018

Chen CK, Zhang YL, Lei P, et al., 2020. A study for predicting the maximum gas temperature beneath ceiling in sealing tactics against tunnel fire. *Tunnelling and Underground Space Technology*, 98:103275. https://doi.org/10.1016/j.tust.2019.103275

Chen CK, Jiao WB, Zhang YL, et al., 2023. Experimental investigation on the influence of longitudinal fire location on critical velocity in a T-shaped tunnel fire. *Tunnelling and Underground Space Technology*, 134:104983. https://doi.org/10.1016/j.tust.2023.104983

Chung CY, Chung PL, 2007. A numerical and experimental study of pollutant dispersion in a traffic tunnel. *Environmental Monitoring and Assessment*, 130(1-3):289-299. https://doi.org/10.1007/s10661-006-9397-0

Gao ZH, Liu MG, Zhao PJ, et al., 2024. Influence of tunnel slope on the one-dimensional spread of smoke transportation and temperature distribution in tunnel fires. *Tunnelling and Underground Space Technology*, 146:105650. https://doi.org/10.1016/j.tust.2024.105650

Gannouni S, Maad RB, 2015. Numerical study of the effect of blockage on critical velocity and backlayering length in longitudinally ventilated tunnel fires. *Tunnelling and Underground Space Technology*, 48:147-155. https://doi.org/10.1016/j.tust.2015.03.003

He K, Cheng XD, Zhang SG, et al., 2018. Critical roof opening longitudinal length for complete smoke exhaustion in subway tunnel fires. *International Journal of Thermal Sciences*, 133:55-61. https://doi.org/10.1016/j.ijthermalsci.2018.07.011

He L, Liao K, Zhou YH, et al., 2023. Study on the influence of the longitudinal position of the fire source on the movement behavior of the asymmetric flow field. *Thermal Science and Engineering Progress*, 39:101753. https://doi.org/10.1016/j.tsep.2023.101753

Ho YT, Kawabata N, Seike M, et al., 2022. Scale model experiments and simulations to investigate the effect of vehicular blockage on backlayering length in tunnel fire. *Buildings*, 12(7):1006. https://doi.org/10.3390/buildings12071006

Hu LH, Huo R, Li YZ, et al., 2005. Full-scale burning tests on studying smoke temperature and velocity along a corridor. *Tunnelling and Underground Space Technology*, 20(3): 223-229. https://doi.org/10.1016/j.tust.2004.08.007

Hu LH, Huo R, Chow WK, 2008. Studies on buoyancy-driven back-layering flow in tunnel fires. *Experimental Thermal and Fluid Science*, 32(8):1468-1483. https://doi.org/10.1016/j.expthermflusci.2008.03.005

Ingason H, Li YZ, 2010. Model scale tunnel fire tests with longitudinal ventilation. *Fire Safety Journal*, 45(6-8): 371-384. https://doi.org/10.1016/j.firesaf.2010.07.004

Ji J, Tan TT, Gao ZH, et al., 2019. Numerical investigation on the influence of length–width ratio of fire source on the smoke movement and temperature distribution in tunnel fires. *Fire Technology*, 55(3):963-979. https://doi.org/10.1007/s10694-018-00814-4

Jiang YQ, Zhang TH, Liu S, et al., 2022. Full-scale fire tests in the underwater tunnel section model with sidewall smoke extraction. *Tunnelling and Underground Space Technology*, 122:104374. https://doi.org/10.1016/j.tust.2022.104374

Khalid S, Wang ZY, Zhou YL, et al., 2023. Numerical modeling on mechanical smoke extraction efficiency of multiple lateral smoke extraction vents system in an immersed tunnel. *International Journal of Thermal Sciences*, 193:108548. https://doi.org/10.1016/j.ijthermalsci.2023.108548

Li LM, Cheng XD, Wang XG, et al., 2012. Temperature distribution of fire-induced flow along tunnels under natural ventilation. *Journal of Fire Sciences*, 30(2):122-137. https://doi.org/10.1177/0734904111428896

Li Q, Kang JH, Wang YN, et al., 2023. Superheated steam similarity simulation on longitudinal distribution of maximum smoke temperature rise in tunnel fires. *Thermal Science and Engineering Progress*, 37:101550. https://doi.org/10.1016/J.TSEP.2022.101550

Li Q, Kang JH, Mei J, 2024. Experimental study on the fire control and smoke transportation using sealing strategy in tunnel. *Tunnelling and Underground Space Technology*, 143:105488. https://doi.org/10.1016/j.tust.2023.105488

Li YZ, Lei B, Ingason H, 2010. Study of critical velocity and backlayering length in longitudinally ventilated tunnel fires. *Fire Safety Journal*, 45(6-8):361-370. https://doi.org/10.1016/j.firesaf.2010.07.003

Liu S, Jiang YQ, Chen JZ, et al., 2016. Full-scale experimental research on the effect of smoke exhaust strategies on efficiency of point extraction system in an underwater tunnel. *Procedia Engineering*, 166:362-372. https://doi.org/10.1016/j.proeng.2016.11.561

Liu SL, Wang L, Yu MG, et al., 2021. Optimization of smoke exhaust efficiency under a lateral central exhaust ventilation mode in an extra-wide immersed tunnel. *Journal of Zhejiang University-SCIENCE A* (*Applied Physics & Engineering*), 22(5):396-406. https://doi.org/10.1631/jzus.A2000336

McGrattan KB, McDermott RJ, Weinschenk CG, et al., 2013. Fire Dynamics Simulator User's Guide. 6th Edition. National Institute of Standards and Technology, USA.

Meng N, Liu BB, Li X, et al., 2018. Effect of blockage-induced near wake flow on fire properties in a longitudinally ventilated tunnel. *International Journal of Thermal Sciences*, 134:1-12. https://doi.org/10.1016/j.ijthermalsci.2018.07.037

Ming YY, Zhu GQ, He L, et al., 2023. Study on smoke flow characteristics in immersed tunnel fires with lateral centralized exhaust: considering the effect of the slope. *Case Studies in Thermal Engineering*, 51:103511. https://doi.org/10.1016/j.csite.2023.103511

Oka Y, Atkinson GT, 1995. Control of smoke flow in tunnel fires. *Fire Safety Journal*, 25(4):305-322. https://doi.org/10.1016/0379-7112(96)00007-0

Se CMK, Lee EWM, Lai ACK, 2012. Impact of location of jet fan on airflow structure in tunnel fire. *Tunnelling and Underground Space Technology*, 27(1):30-40. https://doi.org/10.1016/j.tust.2011.06.005

Tao LL, Zhang YM, Hou KX, et al., 2020. Experimental study on temperature distribution and smoke control in emergency rescue stations of a slope railway tunnel with semi-transverse ventilation. *Tunnelling and Underground Space Technology*, 106:103616. https://doi.org/10.1016/j.tust.2020.103616

Tao LL, Zeng YH, Li J, et al., 2022. Study on the maximum temperature and temperature decay in single-side centralized smoke exhaust tunnel fires. *International Journal of Thermal Sciences*, 172:107277. https://doi.org/10.1016/j.ijthermalsci.2021.107277

Thomas PH, 1958. The movement of buoyant fluid against a stream and the venting of underground fires. *Fire Safety Science*, 1958:351.

Thomas PH, 1968. The movement of smoke in horizontal passages against an air flow. *Fire Safety Science*, 1968:723.

Wang F, Wang MN, Wang QY, 2012. Numerical study of effects of deflected angles of jet fans on the normal ventilation in a curved tunnel. *Tunnelling and Underground Space Technology*, 31:80-85. https://doi.org/10.1016/j.tust.2012.04.009

Weng MC, Lu XL, Liu F, et al., 2016. Study on the critical velocity in a sloping tunnel fire under longitudinal ventilation. *Applied Thermal Engineering*, 94:422-434.

https://doi.org/10.1016/j.applthermaleng.2015.10.059

Xu P, Jiang SP, Xing RJ, et al., 2018. Full-scale immersed tunnel fire experimental research on smoke flow patterns. *Tunnelling and Underground Space Technology*, 81:494-505. https://doi.org/10.1016/j.tust.2018.08.009

Zhang SG, Huang YL, Lin B, et al., 2022. Numerical investigation on the characteristics of lateral smoke extraction in the immersed road tunnel. *Fire and Materials*, 46(8): 1111-1126. https://doi.org/10.1002/fam.3055

Zhang SG, Shi YL, Shi L, et al., 2023. Numerical study on lateral centralized smoke extraction in immersed tunnel with a new-style inclined smoke barrier. *Case Studies in Thermal Engineering*, 42:102770. https://doi.org/10.1016/j.csite.2023.102770

Zhao SZ, Liu F, Wang F, et al., 2018. Experimental studies on fire-induced temperature distribution below ceiling in a longitudinal ventilated metro tunnel. *Tunnelling and Underground Space Technology*, 72:281-293. https://doi.org/10.1016/j.tust.2017.11.032

Zarnaghsh A, Abouali O, Emdad H, et al., 2019. A numerical study of the train-induced unsteady airflow in a tunnel and its effects on the performance of jet fans. *Journal of Wind Engineering and Industrial Aerodynamics*, 187:1-14. https://doi.org/10.1016/j.jweia.2019.01.012

Electronic supplementary materials

Sections S1–S7